Available online at www.sciencedirect.com
ScienceDirect
Fuel 86 (2007) 921–928
FUEL
www.fuelfirst.com

Effect of manganese on an iron-based Fischer–Tropsch synthesis catalyst prepared from ferrous sulfate

Tingzhen Li [a,b], Yong Yang [a], Chenghua Zhang [a], Xia An [a,b], Haijun Wan [a,b], Zhichao Tao [a,b], Hongwei Xiang [a], Yongwang Li [a,*], Fan Yi [c], Binfu Xu [c]

[a] State Key Laboratory of Coal Conversion, Institute of Coal Chemistry, Chinese Academy of Sciences, Taiyuan 030001, PR China
[b] Graduate School of the Chinese Academy of Sciences, Beijing, PR China
[c] College of Physics and Technology, Wuhan University, Wuhan 430072, PR China

Received 23 August 2006; received in revised form 16 October 2006; accepted 29 October 2006
Available online 21 November 2006

Abstract

The effects of manganese on the textural properties, bulk and surface phase compositions, reduction/carburization behaviors and surface basicity of an Fe–Mn–K/SiO_2 catalyst prepared from ferrous sulfate were investigated by N_2 physisorption, Mössbauer spectroscopy, X-ray photoelectron spectroscopy (XPS), H_2 (or CO) temperature-programmed reduction (TPR) and CO_2 temperature-programmed desorption (TPD). The Fischer–Tropsch synthesis (FTS) performance of the catalysts with different contents of manganese was studied in a slurry-phase continuously stirred tank reactor. The characterization results suggested that the added manganese suppressed the crystal growth of hematite and the catalyst reduction from FeO to Fe in H_2. An appropriate amount of manganese improved the FTS activity, increased the surface basicity and enhanced the carburization of the catalyst. However, the excessive addition of manganese retarded the catalyst carburization in CO and syngas due to the high enrichment of manganese on the catalyst surface. At the same time, the addition of manganese suppressed the formation of CH_4 and shifted the selectivity to heavy hydrocarbons (C_{12+}).

Keywords: Fischer–Tropsch synthesis; Iron-based catalyst; Manganese contents

1. Introduction

The Fischer–Tropsch synthesis (FTS) provides a promising route for the production of clean liquid fuels and chemicals from coal and natural gas. The performance of the FTS catalyst plays a critical role in its industrial applications [1]. Presently, only Fe and Co catalysts have been used for industrial FTS. Compared with Co-based catalysts, iron-based catalysts are more suitable for the conversion of syngas with low H_2/CO ratio derived from coal, due to their high FTS activity as well as high water–gas shift (WGS) reactivity, which helps to make up the deficit of H_2 in the syngas [2–4].

It is well known that iron-based catalysts for F–T synthesis are often prepared from iron nitrate [5] and incorporated with certain amounts of potassium, manganese, calcium, zinc, copper and magnesium as promoters to improve its activity and selectivity [6]. Compared with other promoter, manganese shows complex structural and electronic effects. Jaggi et al. [7] studied the effect of manganese content on the phase composition of iron/manganese catalysts and found that a single phase solid solution of Mn in hematite, α-$(Fe_{1-x}Mn_x)_2O_3$, was formed after the catalysts being calcined at 773 K. Similar results have been also reported by Butt [8], Wang et al. [9] and Das et al. [10] over coprecipitated Fe–Mn or Fe–Mn–K catalysts. Besides the formation of solid solution with hematite, manganese can migrate to the catalyst surface during the processes of calcination and reduction [11–14]. Grzybek et al. [11] indicated that the surface enrichment

* Corresponding author. Tel.: +86 351 4130337; fax: +86 351 4050320.
E-mail address: ywl@sxicc.ac.cn (Y. Li).

0016-2361/$ - see front matter © 2006 Elsevier Ltd. All rights reserved.
doi:10.1016/j.fuel.2006.10.019

of manganese was depended on the amount of manganese oxide in the catalyst and the pretreatments temperature, in studying the relationship between the catalyst composition and pretreatment. In addition, Kreitman et al. [12] suggested that the presence of water during the reduction facilitated the enrichment of MnO on the catalyst surface. The study of Leith and Howden [15] over the mixed iron-manganese oxide catalysts revealed that the added of manganese retarded the reduction of iron oxides. Similar results were also obtained by Herranz et al. [16] and Das et al. [10] over unsupported Fe–Mn and Fe–Mn–K catalysts. However, Hughes et al. [13] found that the presence of manganese promoted the reduction of Fe_3O_4 to Fe in studying the manganese promoted iron oxide catalysts. In addition, the suppression effect of manganese on the carburization of iron was reported by Das et al. [17] over iron-based catalysts. However, van Dijk et al. [18] indicated that the presence of manganese had no effect on the catalyst carburization.

The effects of manganese on the FTS performance of iron catalysts have been intensively investigated. Kreitman et al. [12] reported that the manganese-supported iron catalyst showed higher selectivity of lower olefins than that of the un-supported iron catalyst; similar result was also obtained by other groups [9,19,20] over Fe–Mn catalysts. At the same time, the novel effect of manganese on improving the selectivity to lower olefin was also reported over Fe–K [10], Fe/C and Fe–K/C [21], Fe/SiO_2 [17], Fe/Al_2O_3 [22] and $Fe–Mn–K/SiO_2$ [23] catalyst systems. However, van Dijk et al. [18] indicated that no obvious effect on the olefin selectivity was presented for the iron catalysts promoted with manganese. The presence of this controversial result may be due to the different catalyst preparations, pretreatments and FTS conditions. Although the effects of manganese on the performance of iron catalysts have been investigated intensively, little efforts have been performed to illustrate the effects of manganese on the coprecipitated $Fe–Mn–K/SiO_2$ catalyst, especially for the catalyst prepared from ferrous sulfate.

Our group has carried out the study of iron-based FTS catalysts made from ferrous sulfate due to its low cost. The ferrous sulfate solution is firstly oxidized before precipitation. This may result in a more complex structure of the iron catalyst when the manganese promoter is incorporated. Thus, it is necessary to illustrate the effects of manganese on the coprecipitated iron-based catalyst prepared from ferrous sulfate.

The present study aims at a systematic understanding of the promotion effects of manganese on the coprecipitated $Fe–Mn–K/SiO_2$ catalyst prepared from ferrous sulfate under industrially relevant operation conditions. Particular attention is focused on the effect of manganese on the textural properties, reduction, and bulk phase and surface compositions of the catalyst as prepared and after reduction. FTS activity and hydrocarbon product distribution of the catalyst are well correlated with the characterization results.

2. Experimental

2.1. Catalyst preparation

The catalysts used in the present study were prepared using the combination of coprecipitation and spray drying. In brief, a solution containing ferric sulfate derived from the complete oxidation of $FeSO_4 \cdot 7H_2O$ and $MnSO_4 \cdot 6H_2O$ with a desired Fe/Mn weight ratio of $100/x$ ($x = 0$, 7 and 20) was introduced into a 20 l precipitation vessel containing deionized water (~ 1 l) at 353 ± 1 K. A NH_4OH solution was added simultaneously into the vessel to maintain the pH at a constant value of 9.0 ± 0.1. After the precipitation, the precipitate was washed thoroughly with deionized water (323 K) until SO_4^{2-} could not be detected with the $BaCl_2$ solution (0.1 mol/l), and subsequently filtered. The required amount of silica sol, K_2CO_3 solution and deionized water were added into the filter cake to obtain the required $Fe/K/SiO_2$ weight ratio of 100/4/20, and the mixture was then reslurried and spray-dried. The obtained catalyst precursors were calcined at 773 K for 5 h. The compositions of the final obtained catalysts are $100Fe/xMn/4K/20SiO_2$ ($x = 0$, 7 and 20), which are named as Mn-00, Mn-07 and Mn-20, respectively.

2.2. Catalyst characterization

The textural properties (BET surface area, average pore size and pore volume) of fresh catalysts were measured by N_2 physisorption at its normal boiling point (77 K) using a Micromeritics ASAP 2500 system after the catalysts being degassed at 393 K for 6 h.

The surface atomic concentrations of the fresh catalysts were determined by XPS using a PHI Quantera SXM spectrometer with Al Kα radiation and the spectrometer resolution of energy was 0.5 eV. The peak positions were corrected for sample charging by setting the C 1 s binding energy at 284.8 eV. The relative surface concentrations of the elements were determined using the whole peak area of Fe 2p, Mn 2p, K 2p and Si 2p regions and the corresponding sensitivity factors of Wager et al. [24].

The Mössbauer spectra of the catalysts were recorded with a MR 351 constant-acceleration Mössbauer spectrometer (FAST, German) at room temperature, using a 25 mCi ^{57}Co in Pd matrix. The spectrometer was operated in the symmetric constant acceleration mode. The spectra were collected over 512 channels in the mirror image format. Data analysis was performed using a nonlinear least square fitting routine that models the spectra as a combination of singlets, quadruple doublets and magnetic sextuplets based on a Lorentzian line shape profile. The spectral components were identified based on their isomer shift (IS), quadruple splitting (QS), and magnetic hyperfine field (Hhf). All isomer shift values were reported with respect to metallic iron (α-Fe) at the measurement temperature. Magnetic hyperfine fields were calibrated with the 330 kOe field of α-Fe at the ambient temperature.

Temperature-programmed reduction (TPR) studies of the fresh catalysts were performed in a conventional atmospheric quartz flow reactor (5 mm i.d.) using a mixture gas of 5% H_2/95% Ar (H_2-TPR) or 5% CO/95% He (CO-TPR). Typically, 80 mg catalyst was loaded into the reactor and reduced by raising the temperature from 373 K to 1073 K (holding 1073 K for 30 min in H_2-TPR) at a heating rate of 6 K/min. The flow rate of the reduction gas was 50 ml/min in the standard state and the consumption of reduction gas was monitored by the change of thermal conductivity of the effluent gas stream using a thermal conductivity detector (TCD). An in-line liquid-nitrogen trap, located between the reactor and the TCD, was used to continuously remove the water or CO_2 produced during the reduction.

The CO_2-TPD experiment was performed in the same system as used in TPR, with He (50 Nml/min) as the carrier gas. A 200-mg catalyst was loaded into the reactor. Then the catalyst was heated in the carrier gas from 373 K to 773 K (6 K/min), held at 773 K for 60 min, and finally cooled to 373 K for the TPD test. In the subsequent steps, CO_2 adsorption on the catalyst was performed at 373 K for 30 min, and then the catalyst was purged with carrier gas for 60 min to remove the weakly adsorbed CO_2. After this step, CO_2-TPD was carried out while the temperature was increased to 773 K at 6 K/min.

2.3. Reactor system and operation procedure

The FTS performance of the catalysts was tested in a 1 dm^3 continuous slurry tank reactor (CSTR) unit loaded with 20.0 g of catalyst sample and 320 g of liquid paraffin. Detailed description of the reactor and product analysis systems was provided elsewhere [25].

The catalyst was reduced in reactor with syngas (H_2/CO = 1.20) at 553 K, 0.10 MPa, and 1000 h^{-1} for 24 h. After reduction, the reaction system was set to desired reaction conditions of 523 K, 1.5 MPa, H_2/CO = 1.2, and 2000 h^{-1}.

3. Results and discussion

3.1. Textural properties of the fresh catalysts

The textual properties (BET surface area, pore volume and average pore diameter) and elemental compositions in the bulk and the surface of the catalysts are shown in Table 1. It is found that the discrepancy of BET surface area for the catalyst incorporated with different amounts of manganese is not obvious and within the experimental error of the measurement (±3%). Manganese promoter is generally accepted as a structural promoter to improve the dispersion of α-Fe_2O_3 [26]. However, 20 g SiO_2 per 100 g Fe was added into the present catalyst. The added SiO_2 can greatly enhance the dispersion of α-Fe_2O_3, and increase the BET surface area of the catalyst [27]. So the structural effect of manganese promoter is difficult to be distinguished on the SiO_2 supported catalysts only by N_2-physisorption measurement.

Table 1
Textural properties and elemental composition in the bulk and the surface of the fresh catalysts

Catalysts	Mn-00	Mn-07	Mn-20
BET surface area (m^2/g)	192	195	196
Pore volume (cm^3/g)	0.38	0.37	0.32
Average pore size (nm)	8.67	8.33	7.36
Mn/Fe atomic ratio			
Bulk	0	0.07	0.20
Surface	0	0.22	0.64
K/Fe atomic ratio			
Bulk	0.06	0.06	0.06
Surface	0.12	0.09	0.09
Si/Fe atomic ratio			
Bulk	0.19	0.19	0.19
Surface	0.73	0.65	0.58

The results of XPS characterization indicate that the Mn/Fe atomic ratio on the catalyst surface is much larger than that in the bulk, which indicates that manganese enriches on the catalyst surface after the catalyst being calcined. In addition, it is also found that the content of potassium on the catalyst surface decreases gradually with the increase of manganese content.

3.2. Reduction and carburization behaviors

The effect of the manganese promoter on the reduction behavior of the catalysts was measured by H_2-TPR and CO-TPR. The profiles of H_2-TPR and CO-TPR are presented in Figs. 1 and 2, respectively. The amount of H_2 consumed during the different reduction stages is summarized in Table 2. All the catalysts present several reduction peaks. A shoulder peak (600 K) appears and the peak at about 685 K becomes sharp with the addition of manganese. For the manganese-free catalyst (Mn-00), the H_2 consumption of the reduction peak centered at 688 K (0.45 mol H_2/mol Fe) is closed to the theoretical value (0.5 mol H_2/mol Fe) of the reduction of α-Fe_2O_3 to FeO.

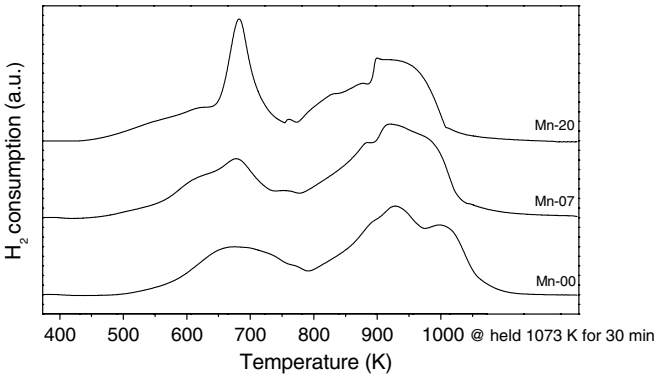

Fig. 1. H_2-TPR profiles of the fresh catalysts.

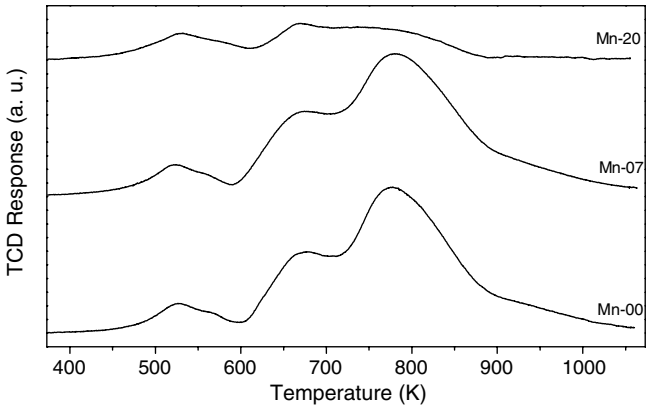

Fig. 2. CO-TPR profiles of the fresh catalysts.

Table 2
Quantitative results of H_2 consumption for the fresh catalysts in H_2-TPR

Catalysts	Peak (K)	H_2 consumption	
		mol H_2/mol M[a]	mol H_2/mol Fe
Mn-00	688	0.45	
	937		0.72
	1026		0.23
Mn-07	614	0.11	
	683	0.33	
	931		0.82
	996		0.12
Mn-20	589	0.13	
	684	0.33	
	858		0.30
	945		0.51

[a] M = Fe + Mn.

Thus, this peak can be assigned to the reduction of α-Fe_2O_3 to FeO. The peaks at 937 K (0.72 mol H_2/mol Fe) and 1026 K (0.23 mol H_2/mol Fe) correspond to the reduction of FeO to Fe. The reduction of α-Fe_2O_3 occurs via FeO as an intermediate phase rather than Fe_3O_4 has also been reported by Zhang et al. [25] and Yang et al. [28] over the silica supported iron-based catalysts. It is known that FeO is a metastable phase of iron oxides below 843 K [29]. FeO as an intermediate phase is observed during the α-Fe_2O_3 reduction, since FeO is stabilized by the support [28]. For the two manganese-promoted catalysts (Mn-07, Mn-20), the reduction peaks at lower temperature (500–800 K) may be assigned to the reduction of the possible solid solution (α-$(Fe_{1-x}Mn_x)_2O_3$) to (Fe,Mn)O, and the peaks at the higher temperature (above 800 K) to the reduction of (Fe,Mn)O to Fe and MnO [7,8,10,19]. The presence of (Fe,Mn)O as the intermediate phase during the reduction may be due to the stabilization effect of manganese and silica [28]. The amount of H_2 consumed during the reduction of (Fe,Mn)O to Fe and MnO (0.94 mol H_2/mol Fe for Mn-07 and 0.81 mol H_2/mol Fe for Mn-20) is less than that of Mn-00 during the reduction of FeO to Fe (0.95 mol H_2/mol Fe), and it decreases with the increase of manganese content, which indicates that the presence of manganese suppresses the catalyst reduction from FeO to Fe. Such a result can be explained as that the formed MnO migrates to the surface of FeO resulting the unreduced FeO encapsulated in MnO [11–14], which causes FeO cannot be further reduced by H_2, during the catalyst reduction from (Fe,Mn)O to Fe and MnO; at the same time, the presence of manganese significantly reduces the hydrogen chemisorption [14].

The CO-TPR profiles of the catalysts are shown in Fig. 2. All the profiles show three peaks. The catalyst is generally reduced and carburized via two steps in CO [25]. The first step at about 523 K presents the reduction of α-$Fe_2O_3 \rightarrow Fe_3O_4$, then the formed Fe_3O_4 is reduced and carburized at the temperature of 600–710 K [25,30,31]. According to the works of Li et al. [30] and Datye et al. [31], the peak at higher temperature (above 710 K) can be ascribed to the deposition of amorphous carbon derived from the Boudouard reaction of CO ($2CO \rightarrow C + CO_2$). The areas of every peak in the CO-TPR profile of Mn-07 are larger than that of Mn-00, which are respectively corresponding to the reduction, carburization and carbon deposition. The result indicates that the addition of a small amount of manganese facilitates the reduction, carburization and carbon deposition of the catalyst in CO. As mentioned above, the addition of a small amount of manganese results in the presence of manganese on the catalyst surface. These manganese atoms on the catalyst surface facilitate the CO chemisorption [14] and promote the catalyst reduction and carburization. Since carbon deposition occurs in parallel with the carbide formation [31], the addition of a small amount of manganese also facilitates the carbon deposition of the catalyst during the CO reduction. With further addition of manganese, the total area of the TPR profile of Mn-20 decreases greatly, which indicates that the addition of a large amount of manganese suppresses the reduction, carburization and carbon deposition of the catalyst. As indicated by the analysis of XPS, the manganese promoter concentrates largely on the catalyst surface. The high enrichment of manganese formed during the calcination and reduction on the catalyst surface reduces the surface concentration of active Fe and results a decrease in CO adsorption [14,32]. Which suppresses the reduction and carburization of the catalyst; at the same time, MnO formed by the reduction of the catalyst does not catalyze the Boudouard reaction of CO [15] and thereby inhibits the carbon deposition of the catalyst in CO-TPR.

3.3. Crystalline structure of the fresh catalysts

The phase composition of the fresh catalysts was measured by Mössbauer spectroscopy. The Mössbauer spectra of the fresh catalysts are shown in Fig. 3, and the parameters derived from the analysis of these spectra are summarized in Table 3. Each catalyst only presents a central doublet. The doublet can be assigned to the superparamagnetic Fe^{3+} ions on the non-cubic sites of α-Fe_2O_3 with the crystallite diameters smaller than 13.5 nm [33,34]. More

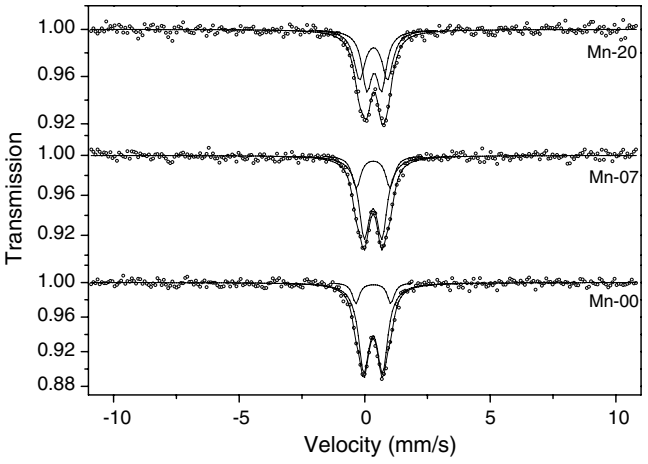

Fig. 3. Mössbauer spectra of the fresh catalysts.

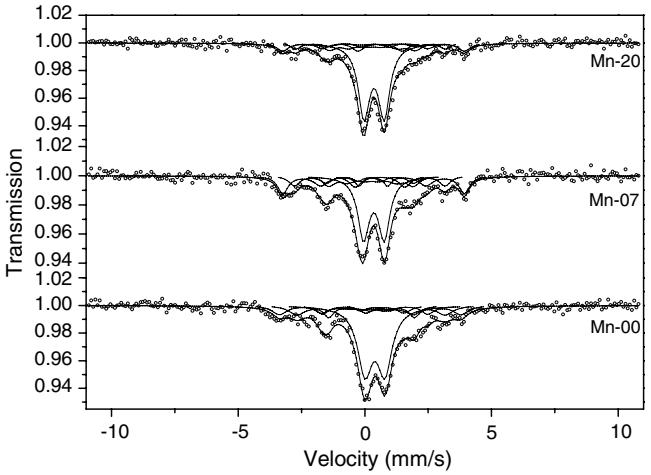

Fig. 4. Mössbauer spectra of the catalysts after reduction. Reduction conditions: 553 K, $H_2/CO = 1.2$, 0.1 MPa and 1000 h^{-1} for 24 h.

precisely, the spectrum can be fitted with two doublets with the same IS values, but different QS values. According to the works of van der Kraan et al. [35,36], low QS values can be attributed to the Fe^{3+} ions within small hematite particles, whereas high QS values can be attributed to the Fe^{3+} ions on the surface of such particles. The average crystallite size (d_p) can be estimated on the basis of Mössbauer measurements [37,38]. It is found that the average crystallite diameter of α-Fe_2O_3 decreases with the increase of manganese content. The result indicates that the addition of manganese improves the dispersion of α-Fe_2O_3 and reduces the α-Fe_2O_3 particle size, which confirms the results of N_2 physisorption. Similar result that the addition of manganese can improve the dispersion of iron oxides by reducing their particle size has been reported by Das et al. [17] over the silicalite-1 supported Fe–Mn catalysts. Furthermore, the increased quadruple splitting (QS) of the doublet with the increase of manganese content implies that part of manganese atoms entrance cubic symmetrical sites of α-Fe_2O_3 crystallite lattice [33], since the quadruple splitting of spm α-Fe_2O_3 increases with the decrease in symmetry of crystallite lattice.

3.4. Crystalline structure of the catalysts after reduction

The Mössbauer spectra of the catalysts with different manganese contents after being reduced with syngas ($H_2/CO = 1.2$) at 553 K, 0.1 MPa and 1000 h^{-1} for 24 h are presented in Fig. 4, and the phase compositions of the catalysts determined by fitting the Mössbauer spectra are listed in Table 4. All the catalysts are mainly composed

Table 4
Mössbauer parameters of the catalysts after reduction

Catalysts	Assignment	Mössbauer parameters			
		IS (mm/s)	QS (mm/s)	Hhf (kOe)	Area (%)
Mn-00	χ-Fe_5C_2	0.31	−0.20	223	15.6
		0.25	−0.02	182	17.1
		0.29	−0.37	113	10.6
	Fe^{2+}	0.79	1.50		5.6
	Fe^{3+}	0.40	0.78		51.1
Mn-07	χ-Fe_5C_2	0.34	0.01	223	23.2
		0.20	−0.01	185	13.7
		0.26	−0.03	104	14.3
	Fe^{2+}	0.60	1.96		8.1
	Fe^{3+}	0.36	0.82		40.7
Mn-20	χ-Fe_5C_2	0.37	−0.06	223	12.2
		0.25	−0.06	183	8.0
		0.32	−0.04	105	10.7
	Fe^{2+}	0.60	1.74		8.0
	Fe^{3+}	0.36	0.80		61.1

Reduction conditions: 553 K, $H_2/CO = 1.2$, 0.1 MPa and 1000 h^{-1} for 24 h.

Table 3
Mössbauer parameters of the fresh catalysts

Catalysts	Assignment	Mössbauer parameters				
		IS (mm/s)	QS (mm/s)	FWHM (mm/s)	Area (%)	Average d_p[a] (nm)
Mn-00	Fe^{3+} (spm in bulk)	0.34	0.65	3.05	85.9	5.5
	Fe^{3+} (spm in surface)	0.34	1.31	1.96	14.1	
Mn-07	Fe^{3+} (spm in bulk)	0.35	0.70	3.05	74.3	2.6
	Fe^{3+} (spm in surface)	0.35	1.35	2.47	25.7	
Mn-20	Fe^{3+} (spm in bulk)	0.38	0.73	2.80	50.0	0.9
	Fe^{3+} (spm in surface)	0.35	1.36	3.19	50.0	

D = 'atoms located in the "bulk" of the crystallites'/'atoms located on the "surface" of the crystallites'.
[a] $d_p = 0.9/D$.

of superparamagnetic Fe^{2+}, Fe^{3+} ions and χ-Fe_5C_2 after the reduction. The catalyst of Mn-07 has the largest amount of iron carbides. However, Mn-20 has the least amount of iron carbides. As mentioned above, the addition of a small amount of manganese reduces the crystallite size of α-Fe_2O_3 and thereby promotes the catalyst reduction and carburization; however, when the catalyst contains a large amount of manganese, the high enrichment of manganese on the catalyst surface suppresses the reduction and carburization of the catalyst in syngas, which is well agreed with the results of the CO-TPR study mentioned above.

3.5. Surface basicity

The effect of manganese on the surface basicity of the catalysts was studied by CO_2-TPD. The CO_2-TPD profiles are presented in Fig. 5. A small peak (peak 1) at about 400 K and a long tail peak (peak 4) at temperature above 610 K are presented in all of the profiles. The small peak at low temperature may be attributed to the desorption of the weakly adsorbed CO_2, and the tail peak is probably due to the decomposition of a small amount of metal carbonates formed during the CO_2 adsorption or catalyst preparation [25]. Peaks 2 and 3 presented in the TPD profiles of the catalysts correspond to desorption of CO_2 that interacts with surface basic sites. Compared with Mn-00, peak 2 of Mn-07 shifts to higher temperature and becomes stronger, whereas peak 3 shifts to lower temperature. With the further increase of manganese content, for Mn-20, peak 2 becomes weaker and peak 3 shifts further to lower temperature. In addition, the total area of the TPD profile of the catalyst promoted with manganese is larger than that of the un-promoted catalyst. The result indicates that the presence of manganese improves the catalyst surface basicity. This result can be ascribed to the fact that the enrichment of manganese oxide on the catalyst surface improves the catalyst surface basicity, since manganese oxide alone exhibits surface basicity [39], and the surface basicity of manganese oxide is stronger than that of iron oxide [14]. However, the total area of the TPD profile of Mn-20 is smaller than that of Mn-07, which indicates that the addition of a large amount of manganese decreases the catalyst surface basicity. The high enrichment of manganese on the surface of the catalyst contained a large amount of manganese decreases the surface effective potassium content greatly and thereby decreases the catalyst surface basicity, since the catalyst surface basicity is mainly from K-basic sites when the catalyst is promoted with potassium [25]. The result of XPS analysis above supports the fact that the addition of a large amount of manganese reduces greatly the content of potassium on the catalyst surface.

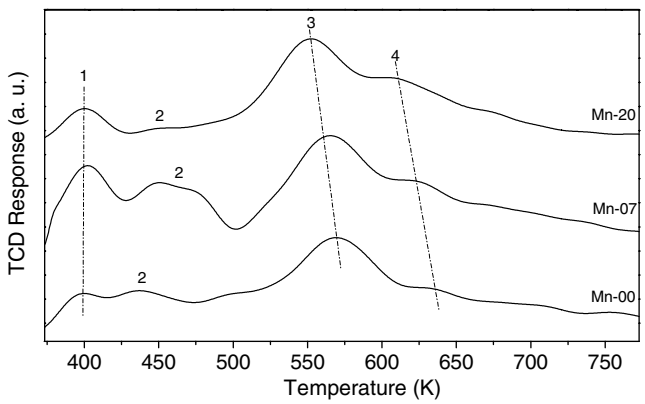

Fig. 5. CO_2-TPD profiles of the fresh catalysts.

3.6. FTS performance

FTS performance of the catalysts with different manganese contents was measured in a CSTR system under conditions of 523 K, 1.5 MPa, 2000 h^{-1} and $H_2/CO = 1.2$.

3.6.1. Activity and stability

The effect of manganese on the FTS activity measured with CO conversion of the catalysts is shown in Fig. 6. The CO conversion of Mn-00 increases slowly with time on stream and approaches the steady state after a long induction period (400 h). Before approaching the steady state, Mn-07 has a 150 h induction period. However, Mn-20 almost has no induction period. The decrease of the induction period of the catalysts suggests that the presence of manganese increases the rates of reduction and carburization of the catalysts when syngas is used as the reduction gas. After approaching the steady state, Mn-07 has the highest CO conversion, whereas Mn-20 has the lowest value. As indicated by the Mössbauer spectra measurement of the catalysts reduced by syngas, Mn-07 has the largest amount of iron carbides, whereas Mn-20 has the least amount of iron carbides. The catalyst with higher carburization extent has higher activity. Since iron carbides are generally considered as the active phases for FTS [40–42].

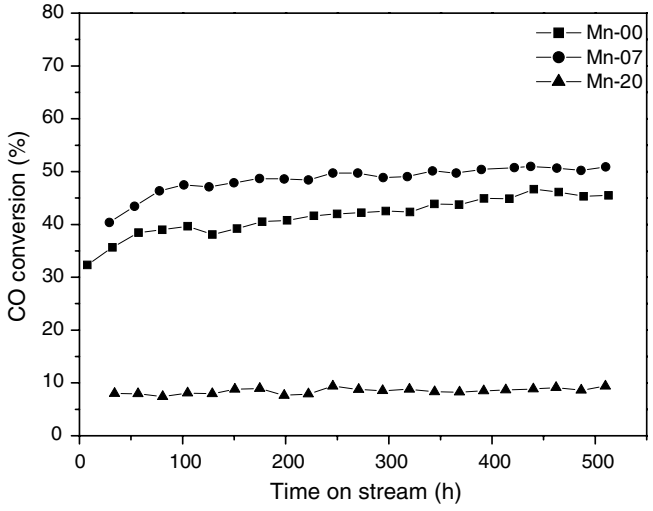

Fig. 6. CO conversion and stability of the catalysts. Reaction conditions: 523 K, 1.5 MPa, 2000 h^{-1}, and $H_2/CO = 1.2$.

Table 5
Hydrocarbon selectivity of the catalysts

Catalyst time on stream (h)	Mn-00		Mn-07		Mn-20	
	203	513	198	510	199	510
CO conversion (%)	41.7	45.9	48.1	51.2	8.9	9.4
H_2 conversion (%)	40.4	42.3	44.8	46.1	12.5	12.3
$CO + H_2$ conversion (%)	41.0	44.0	46.3	48.4	10.8	11.0
$n(H_2)/n(CO)$ in tail gas	1.23	1.28	1.28	1.33	1.15	1.16
HC distribution (wt.%)						
CH_4	9.6	9.6	9.1	9.5	4.4	4.7
C_2–C_4	39.1	38.6	34.0	34.3	23.4	23.3
$C_2^=$–$C_4^=$	29.8	28.9	26.8	26.4	19.9	20.0
C_2^0–C_4^0	9.3	9.7	7.2	7.8	3.5	3.3
$n(C_2^=–C_4^=)/n(C_2^0–C_4^0)$	3.2	3.0	3.7	3.4	5.8	6.1
C_5–C_{11}	41.2	38.1	36.9	32.2	28.5	28.7
C_{12+}	10.1	13.7	20.0	24.1	43.7	43.4
α_1/α_2[a]	0.62/0.69	0.62/0.76	0.62/0.78	0.60/0.82	0.60/0.90	0.57/0.89

Reaction conditions: 523 K, 1.5 MPa, 2000 h^{-1}, and $H_2/CO = 1.2$.
[a] α_1 and α_2 are growth probabilities in carbon number ranges of C_3–C_8 and C_{10}–C_{20}, respectively.

3.7. Selectivity

Typical data of FTS activity, H_2/CO ratio in tail gas and hydrocarbon distribution of the catalysts are summarized in Table 5. The selectivity to light hydrocarbons (CH_4, C_2–C_4, and C_5–C_{11}) is suppressed with the addition of manganese into the catalyst. The suppression effect of manganese on the formation of CH_4 has also been reported by Barrault et al. [20]. However, the selectivity to heavy hydrocarbons (C_{12+}) and the $C_2^=–C_4^=/C_2^0–C_4^0$ ratio are enhanced with the addition of manganese. It is well known that increasing the surface basicity of an FTS catalyst can improve the CO dissociative adsorption, suppress the H_2 adsorption, facilitate the chain growth reaction, and enhance the selectivity to heavy hydrocarbons [39,43]. As discussed above, the catalyst surface basicity is enhanced by the presence of manganese. Thus, the suppression effect on the formation of light hydrocarbons and the enhancement of the selectivity to heavy products can be ascribed to the enhancement of the surface basicity of the catalysts with the presence of manganese. The CO_2-TPD study also indicates that the surface basicity of Mn-07 is stronger than that of Mn-20. However, the selectivity to heavy hydrocarbons of Mn-07 is lower than that of Mn-20. It is known that the reaction conditions also influence the FTS selectivity besides the catalyst itself. The H_2/CO ratio has the strongest influence [44]. As shown in Table 5, the H_2/CO ratio in tail gas of Mn-07 is much higher than that of Mn-20. Therefore, the fundamental reason of this phenomenon is that the higher H_2/CO ratio in the reaction atmosphere suppresses the chain growth and the formation of heavy products [26].

4. Conclusion

The effects of manganese promoter on iron-based FTS catalysts prepared from ferrous sulfate were systemically studied. The catalyst promoted with manganese has small α-Fe_2O_3 crystallite size. The content of manganese on the surface of the fresh catalysts is much larger than that in the bulk, since Mn immigrated to the surface during the calcination. The added manganese suppresses the catalyst reduction from FeO to Fe in H_2. The addition of an appropriate amount of manganese promotes the catalyst reduction and carburization in syngas and CO. However, the excessive addition of manganese suppresses the catalyst reduction and carburization due to its high enrichment on the catalyst surface. The incorporation of a small amount of manganese can greatly increase the catalyst surface basicity. However, the excessive addition of manganese only has a slight effect on the surface basicity, since the high enrichment of manganese decreases the effective potassium content on the catalyst surface. The catalyst Mn-07 ($100Fe/7Mn/4K/20SiO_2$) has the maximum catalytic activity in FTS. It is found that the addition of manganese suppresses the formation of CH_4 and promotes the selectivity to heavy hydrocarbons.

Acknowledgements

We thank the financial support from the National Natural Science Foundation of China (20590360) and Natural Science Foundation of Shanxi (2006021014).

References

[1] Dry ME. Appl Catal A 2004;276:1–3.
[2] Dry ME. Catal Today 2002;71:227–41.
[3] Dry ME. J Chem Technol Biot 2001;77:43–50.
[4] Yang Y, Xiang H, Zhang R, Zhong B, Li Y. Catal Today 2005;106: z170–5.
[5] Wu B, Tian L, Xiang H, Zhang Z, Li YW. Catal Lett 2005;102:211–8.
[6] Yang Y, Xiang H, Xu Y, Bai L, Li Y. Appl Catal A 2004;266:181–94.
[7] Jaggi NK, Schwartz LH, Butt JB. Appl Catal 1985;13:347–61.
[8] Butt JB. Catal Lett 1990;7:83–106.
[9] Wang C, Wang Q, Sun X, Xu L. Catal Lett 2005;105:93–101.
[10] Das CK, Das NS, Choudhury DP, Ravichandran G, Chakrabarty DK. Appl Catal A 1994;111:119–32.

[11] Grzybek T, Papp H, Baerns M. Appl Catal 1987;29:335–50.
[12] Kreitman KM, Baerns M, Butt JB. J Catal 1987;105:319–34.
[13] Hughes ISC, Newman JOH, Bond GC. Appl Catal 1987;30:303–11.
[14] Jensen KB, Massoth FE. J Catal 1985;92:98–108.
[15] Leith IR, Howden MG. Appl Catal 1988;37:75–92.
[16] Herranz T, Rojas S, Pérez-Alonso FJ, Ojeda M, Terreros P, Fierro JLG. Appl Catal A 2006;311:66–75.
[17] Das D, Ravichandran G, Chakrabarty DK. Catal Today 1997;36: 285–93.
[18] Van Dijk WL, Niemantsverdriet JW, Van der Kraan AM, Van der Baan HS. Appl Catal 1982;2:273–88.
[19] Maiti GC, Malessa R, Löchner U, Papp H, Baerns M. Appl Catal 1985;16:215–25.
[20] Barrault J, Forquy C, Perrichon V. Appl Catal 1983;5:119–25.
[21] Venter J, Kaminsky M, Geoffroy GL, Vannice MA. J Catal 1987;105: 155–62.
[22] Abbot J, Clark NJ, Baker BG. Appl Catal 1986;26:141–53.
[23] Xu L, Wang Q, Xu Y, Huang J. Catal Lett 1995;31:253–66.
[24] Wagner CD, Davis LE, Zeller MV, Taylor JA, Raymond RH, Gale LH. Surf Interface Anal 1981;3:211–25.
[25] Zhang CH, Yang Y, Teng BT, Li TZ, Zheng HY, Xiang HW, et al. J Catal 2006;237:405–15.
[26] Bai L, Xiang HW, Li YW, Han YZ, Zhong B. Fuel 2002;81: 1577–1581.
[27] Wan HJ, Wu BS, Tao ZC, Li TZ, An X, Xiang HW, et al. J Mol Catal A 2006;260:255–63.
[28] Yang Y, Xiang HW, Tian L, Wang H, Zhang CH, Tao ZC, et al. Appl Catal A 2005;284:105–22.
[29] Kock AJHM, Fortuin HM, Geus JW. J Catal 1985;96:261–75.
[30] Li S, Li A, Krishnamoorthy S, Iglesia E. Catal Lett 2001;77:197–205.
[31] Jin Y, Datye AK. J Catal 2000;196:8–17.
[32] Jensen KB, Massoth FE. J Catal 1985;92:109–18.
[33] Kolk B, Albers A, Leith IR, Howden MG. Appl Catal 1988;37:57–74.
[34] Kündig W, Bömmel H, Constabaris G, Lindquist RH. Phys Rev 1966;142:327–33.
[35] Van der Kraan AM. Phys. Status Solidi A 1973;18:215–26.
[36] Van den Berg FR, Crajé MWJ, Van der Kraan AM, Geus JW. Appl Catal A 2003;251:347–57.
[37] Dlamini H, Motjope T, Joorst G, Ter Stege G, Mdleleni M. Catal Lett 2002;78(1–4):201–7.
[38] Lox ES, Marin GB, De Grave E, Bussière P. Appl Catal 1988;40: 197–218.
[39] Dry ME, Oosthuizen GJ. J Catal 1968;11:18–24.
[40] Motjope TR, Dlamini HT, Hearne GR, Coville NJ. Catal Today 2002;71:335–41.
[41] Mansker LD, Jin Y, Bukur DB, Datye AK. Appl Catal A 1999;186: 277–96.
[42] Li S, Krishnamoorthy S, Li A, Meitzner GD, Iglesia E. J Catal 2002; 206:202–17.
[43] Miller DG, Moskovits M. J Phys Chem 1988;92:6081–5.
[44] Ji YY, Xiang HW, Yang JL, Xu YY, Li YW, Zhong B. Appl Catal A 2001;214:77–86.